Available online at www.sciencedirect.com
SCIENCE DIRECT
C. R. Mecanique 333 (2005) 856–866
COMPTES RENDUS MECANIQUE
http://france.elsevier.com/direct/CRAS2B/

Fluid–solid interactions: modeling, simulation, bio-mechanical applications

A three-dimensional fluid–structure interaction method for heart valve modelling

Raoul van Loon [a,1], Patrick D. Anderson [b], Frank P.T. Baaijens [a], Frans N. van de Vosse [a,*]

[a] *Department of Biomedical Engineering, Eindhoven University of Technology, P.O. Box 513, 5600 MB, Eindhoven, The Netherlands*
[b] *Department of Mechanical Engineering, Eindhoven University of Technology, P.O. Box 513, 5600 MB, Eindhoven, The Netherlands*

Abstract

A method is presented for modelling fluid–solid interaction with large transformations of a slender solid body. The fluid flow is described by the unsteady Navier–Stokes equation, and the solid deformation is described by an incompressible hyperelastic Neo-Hookean model. Although the fluid and solid mesh are non-conformal with respect to each other, both domains can be coupled using a Lagrange multiplier. Accuracy and robustness are improved by a computationally inexpensive adaptive meshing scheme which is applied to the fluid mesh at the position of the solid interface. To illustrate the applicability of this method, 2D and 3D model problems are presented that are closely related to dynamical heart-valve computations. ***To cite this article: R. van Loon et al., C. R. Mecanique 333 (2005).***

Résumé

Une méthode de couplage fluide–structure pour la modélisation numérique en trois dimensions des valves cardiaques. Dans cet article, on présente une méthode pour la modélisation numérique de couplages fluide–solide lorsque le solide est un corps mince. L'écoulement est décrit par les équations de Navier–Stokes instationnaires, la déformation du solide l'étant par un modèle du type Neo-Hookien hyper élastique incompressible. Bien que les maillages fluide et solide ne soient pas en conformité, l'un par rapport à d'autres on peut coupler les regions respectives via un multiplicateur de Lagrange. Par rapport à d'autres approches de ce type, on améliore précision et robustesse par l'utilisation d'une méthode de maillage adaptative, peu coûteuse, appliquée au maillage fluide au voisinage de l'interface avec le solide. Pour évaluer les possibilités de la méthode, on l'applique à la résolution de problèmes modèles, bi et tri-dimensionnels, tous étroitement liés à la simulation numé rique du mouvement des valves cardiaques en régîme dynamique. ***Pour citer cet article : R. van Loon et al., C. R. Mecanique 333 (2005).***

Keywords: Computational fluid mechanics; Heart valves; Fictitious domains; Adaptive meshing; Fluid–structure; Lagrange multipliers

Mots-clés : Mécanique des fluides numérique ; Valves cardiaques ; Domaines fictifs ; Maillages adaptatifs ; Couplage fluide–structure ; Multiplicateurs de Lagrange

* Corresponding author.
E-mail addresses: R.v.loon@tue.nl (R. van Loon), F.N.v.d.Vosse@tue.nl (F.N. van de Vosse).
[1] Contract/grant sponsor: Hemodyn; contract/grant number TSGE-1054.

1631-0721/$ – see front matter
doi:10.1016/j.crme.2005.10.008

1. Introduction

Many attempts have been made to capture the dynamics of an aortic heart valve, but although progress is booked in the past, still no models are available for computing one or more cardiac cycles with a realistic three-dimensional geometry and realistic material parameters. Many techniques are involved in modelling this problem. The model should incorporate large rotations, translations and deformations of the valve. Furthermore, the compliant aortic root, to which the valve is attached, influences the opening and closing behaviour of the three leaflets by transient variations in radius. In order to capture closure of the valve, a contact algorithm should be incorporated into the model and finally, the interaction between blood and valve should be addressed.

A first attempt in modelling this fluid–structure problem was taken by Peskin [1] introducing a method which is now known as the Immersed Boundary Method [2]. In an Eulerian–Lagrangian framework, the valve was represented, introducing a set of points, in which forces were imposed on the fluid domain. The points were interconnected by a generalised Hooke's law and were able to move across the fixed fluid mesh. This method was extended for 3D problems and applied to several valve and heart simulations in e.g. [3,4]. Makhijani et al. [5] also proposed a three-dimensional model in which fluid and solid were solved fully coupled. They used a combination of an Arbitrary Lagrangian Eulerian approach (ALE) and remeshing for describing the large movements of the solid. In an ALE method as exploited by e.g. [6–8], the Eulerian grid is translated according to the movement of a Lagrangian grid and is corrected by taking into account the grid velocity in the convective term. Since the shape of the elements in the Eulerian grid degenerates in case of large solid body translations, a combination with remeshing is needed. A finite volume method was used for the fluid and combined with a finite element method for the solid. A finite element model of a 3D patient specific aortic root and valve was presented by Nicosia et al. [9]. The computations were performed in an uncoupled manner and included the opening and closing behaviour. The aortic valve and root were modelled using Hughes–Liu shell elements with linear elastic material behaviour. For stability reasons the peak diastolic pressure was reduced.

Recently, a fully coupled 3D model of an aortic root and valve was published by De Hart et al. [10–12]. In this approach fluid and solid were described in an Eulerian and Lagrangian framework, respectively, and coupled using a Lagrange multiplier. This variation of the fictitious domain approach, as exploited in e.g. [13,15,17,16,14], considers a fictitious solid domain immersed in a fluid domain, with meshes that are non-conformal with respect to each other. The influence of a stented valve [10], a stentless valve [11] and constitutive behaviour of the solid [12] on the solid movement and deformation was analysed. In this last work the influence of a fiber reinforced hyper elastic Neo-Hookean material law representing the leaflet structure of collagen fibers and matrix material was analysed. Although this fluid–structure interaction method looks promising with respect to the solid movement during systole, capturing the transvalvular pressure drop during diastole is still a problem. In the work of Stijnen et al. [18] this problem was overcome for a stiff mechanical valve. By introducing an inner fluid curve that coincides with the position of the solid boundary at the moment of closure, the coupling between fluid and solid is strong enough to describe a pressure drop in the fluid. Van Loon et al. [19] extended this approach for flexible solid structures by introducing a local fluid mesh adaptation which provides for the creation of this inner fluid curve every time step. This method has the additional advantage that shear stresses can be computed at both sides of the solid.

In this article the method as proposed by Van Loon [19] is extended to 3D. Furthermore, the adaptive meshing algorithm has changed in the sense that the fluid mesh does not keep its topology anymore, which improves the methods robustness in 3D. First the governing equations will be given after which the adaptive meshing algorithm is treated. Finally, several model problems in 2D and 3D are presented which address the potential of the method.

2. Mathematical formulation

2.1. Governing equations

2.1.1. Fluid

Consider a fluid domain Ω^f with the governing equations for the fluid given by the unsteady Navier–Stokes equation. The balance of momentum, continuity equation and constitutive law then read,

$$\rho\left(\frac{\partial \boldsymbol{u}^f}{\partial t} + \boldsymbol{u}^f \cdot \boldsymbol{\nabla}\boldsymbol{u}^f\right) = \boldsymbol{\nabla}\cdot\boldsymbol{\sigma}^f \quad \text{in } \Omega^f \tag{1}$$

$$\boldsymbol{\nabla}\cdot\boldsymbol{u}^f = 0 \quad \text{in } \Omega^f \tag{2}$$

$$\boldsymbol{\sigma}^f = 2\eta\boldsymbol{D} - p^f\boldsymbol{I}, \quad \text{with } \boldsymbol{D} = \frac{1}{2}\left(\boldsymbol{\nabla}\boldsymbol{u}^f + \left(\boldsymbol{\nabla}\boldsymbol{u}^f\right)^{\mathrm{T}}\right) \tag{3}$$

with ρ, η, $\boldsymbol{u}^f$, p^f, and $\boldsymbol{I}$ the density, dynamic viscosity, unity tensor, fluid velocity and fluid pressure, respectively. The gradient operators with respect to the reference and current configuration are denoted by $\boldsymbol{\nabla}_0$ and $\boldsymbol{\nabla}$, respectively. Symbols with respect to the fluid will be denoted with ^{f} in this paper. Since modelling of the pulsatile blood flow in the aortic root is our goal, inertia and convection terms cannot be neglected, because the physiological Strouhal (*Sr*) and Reynolds (*Re*) number read approximately 0.06 and 4500 in this region of the arterial tree. Note that, although blood shows a non-Newtonian behaviour, it will be modelled as a Newtonian fluid since it is not of importance for the models presented in this work.

2.1.2. Solid

Next the solid domain Ω^s is considered. The theory in this article is developed for fluid–structure interaction problems concerning flexible solids. Hence, deformations are too large to use an infinitesimal theory leading us to choose a hyperelastic, Neo-Hookean constitutive model for describing the solid behaviour:

$$\boldsymbol{\nabla}\cdot\boldsymbol{\sigma}^s = \boldsymbol{0} \quad \text{in } \Omega^s \tag{4}$$

$$\det(\boldsymbol{F}) = 1 \quad \text{in } \Omega^s \tag{5}$$

$$\boldsymbol{\sigma}^s = G\left(\boldsymbol{F}\cdot\boldsymbol{F}^{\mathrm{T}} - \boldsymbol{I}\right) - p^s\boldsymbol{I} \quad \text{with } \boldsymbol{F} = (\boldsymbol{\nabla}_0\boldsymbol{x})^{\mathrm{T}} \tag{6}$$

The quantities $\boldsymbol{x}$, p^s and G denote the position, pressure and shear modulus, respectively. The superscript ^{s} will be used to denote the solid. Since heart valves are neutrally buoyant, gravity effects can be neglected. Furthermore, the inertia and convection term in the solid are neglected with respect to the elastic term. In the scope of this paper, it is not necessary to model the complex material structure and behaviour typical for heart valves. A homogeneous, isotropic material law is sufficient for the purpose of presenting the fluid–structure interaction method.

2.1.3. Fluid–structure coupling

Finally, the coupling between fluid domain Ω^f and the imbedded solid domain Ω^s is considered. The interaction between fluid and solid is modelled by applying a no-slip condition $\boldsymbol{u}^f - \boldsymbol{u}^s = \boldsymbol{0}$ at the boundary of the solid. Eqs. (1) and (4) are coupled by applying this constraint in a 'weak' manner, by means of a Lagrange multiplier. This multiplier is defined over a surface γ^f, where integrals over fluid and solid velocity are forced to be equal, namely

$$\int_{\gamma^f} \boldsymbol{q}^\lambda \cdot \left(\boldsymbol{u}^f - \boldsymbol{u}^s\right) \mathrm{d}\gamma^f = 0 \tag{7}$$

where $\boldsymbol{q}^\lambda$ is a trial function. Note that γ^f is defined along the boundary of the solid such that $\gamma^f \subset \Omega^s$, but also $\gamma^f \subset \Omega^f$. In this light the physical meaning of the multiplier is the traction force between the fluid and the solid. For a more extensive discussion on the weak formulation and the exact coupling of solid and fluid, the reader is referred to [16,19].

2.2. Discretisation

The solid domain, fluid domain and Lagrange multiplier domain now need to be discretised. In this section three-dimensional domains for fluid and solid are considered. However, with respect to the two-dimensional model problems in the next section, the approach treated in this section can easily be reduced to the two-dimensional case.

For convenience, we will first introduce some definitions concerning the mesh. Noting that the boundary of a domain will be indicated by the prefix ∂, we consider an open domain $\Omega \subset \mathbb{R}^3$ and its boundary $\partial\Omega \subset \mathbb{R}^3$. This domain can be subdivided into N_Ω elements Ω_e, and the corresponding elemental faces Λ_i, edges Γ_j and nodes n_k, such that,

$$\overline{\Omega} = \bigcup_{e=1}^{N_\Omega} \overline{\Omega}_e, \qquad {}^{\Omega}S = \{e \in \mathbb{N}\colon\ \Omega_{e\neq i} \cap \Omega_i = \emptyset\}, \quad \forall i \in \mathbb{N}$$

$$\partial\Omega_e = \bigcup_{i=1}^{N_\Lambda} {}_e\bar{\Lambda}_i, \qquad {}^{\Lambda}S = \{k \in \mathbb{N}\colon\ \Lambda_k = {}_e\Lambda_i,\ \Lambda_{k\neq l} \cap \Lambda_l = \emptyset\}, \quad \forall {}_e\Lambda_i,\ \forall l \in \mathbb{N}$$

$$\partial\Lambda_i = \bigcup_{j=1}^{N_\Gamma} {}_i\overline{\Gamma}_j, \qquad {}^{\Gamma}S = \{k \in \mathbb{N}\colon\ \Gamma_k = {}_i\Gamma_j,\ \Gamma_{k\neq l} \cap \Gamma_l = \emptyset\}, \quad \forall {}_i\Gamma_j,\ \forall l \in \mathbb{N}$$

$$\partial\Gamma_j = \bigcup_{k=1}^{N_x} x_k, \qquad {}^{x}S = \{k \in \mathbb{N}\colon\ x_{k\neq l} \neq x_l\},\ \forall l \in \mathbb{N}$$

where N_Λ is the number of faces per element, N_Γ is the number of edges per face and N_x is the number of nodal points per edge. The above states that elements in the mesh are non-overlapping and all edges and faces are straight, except for $\Gamma_i \subset \partial\Omega$ and $\Lambda_i \subset \partial\Omega$, which can be curved. A local variable is denoted using two subscripts like ${}_i\Gamma_j$, while a global variable is denoted using only one subscript like Γ_i. The sets ${}^{\Omega}S$, ${}^{\Lambda}S$, ${}^{\Gamma}S$ and ${}^{x}S$ consist of all global elements, faces, edges and nodal numbers, respectively.

Now that definitions with respect to the mesh are made, domains $\Omega^f \subset \mathbb{R}^3$ and $\Omega^s \subset \mathbb{R}^3$ can be discretised in their initial configurations independently from one another to obtain the conformal meshes ${}^{\Omega}S^f$ and ${}^{\Omega}S^s$, respectively. Mesh ${}^{\Omega}S^f$ consists of tetrahedral elements and ${}^{\Omega}S^s$ consists of hexahedral elements.

2.2.1. Adaptive meshing

In the following, a procedure is introduced for adapting the fluid mesh based on the position of the solid mesh. Note that this procedure is only applicable if ${}^{\Omega}S^f$ consists of tetrahedral elements. The shape of elements in ${}^{\Omega}S^s$, however, can be chosen arbitrarily. The objective of adapting the mesh is to create a surface $\gamma^f \subset \Omega^f$ at which the fluid and solid will be coupled.

Consider the solid domain Ω^s and fluid domain Ω^f such that $\Omega^s \cap \Omega^f \neq \emptyset$. An arbitrary surface in the solid domain can now be chosen as a collection of N^s elemental faces,

$$\gamma^s = \bigcup_{i=1}^{N^s} \bar{\Lambda}_i^s \quad \text{with } i \in {}^{\Lambda}S^s$$

at which coupling between fluid and solid should be established. The fluid mesh will be adapted based on the position of boundary γ^s. Therefore, a set of edges that intersect boundary γ^s and the corresponding intersection points can be defined as,

$$S^f = \left\{i \in {}^{\Gamma}S^f\colon\ \overline{\Gamma}_i^f \cap \gamma^s \neq \emptyset,\ \overline{\Gamma}_i^f \cap \gamma^s \neq \overline{\Gamma}_i^f\right\}$$
$$X_i = \left\{\boldsymbol{x}\colon\ \boldsymbol{x} \in \overline{\Gamma}_i^f \cap \gamma^s\right\} \quad \forall i \in S^f$$

Thus, the points found in X_i are the intersection points of a fluid edge $\overline{\Gamma}_i^f$ with γ^s. If X_i contains more than one intersection point, only one, arbitrarily chosen, point is taken into account in the rest of this adaptive meshing algorithm. A parameter ϵ_i is introduced such that,

$$\epsilon_i = \frac{\|\boldsymbol{x}_i - \boldsymbol{x}_{n_{1,i}}\|}{\|\boldsymbol{x}_{n_{2,i}} - \boldsymbol{x}_{n_{1,i}}\|}, \quad \forall \boldsymbol{x}_i \in X_i$$

where the begin node and end node of edge $\overline{\Gamma}_i^f$ are indicated by $n_{1,i} \in {}^{x}S^f$ and $n_{2,i} \in {}^{x}S^f$. If the length of edge Γ_i^f is defined as $\|\Gamma_i^f\| \equiv \|\boldsymbol{x}_{n_{2,i}} - \boldsymbol{x}_{n_{1,i}}\|$, it can be stated that, $\forall\epsilon_i$,

$$S^{f1} = \left\{i \in S^f\colon\ \epsilon_i < \hat{\epsilon}\left\|\Gamma_i^f\right\|\right\}$$
$$S^{f2} = \left\{i \in S^f\colon\ \epsilon_i > (1-\hat{\epsilon})\left\|\Gamma_i^f\right\|\right\}$$
$$S^{f3} = \left\{i \in S^f\colon\ \hat{\epsilon}\left\|\Gamma_i^f\right\| < \epsilon_i < (1-\hat{\epsilon})\left\|\Gamma_i^f\right\|\right\}$$

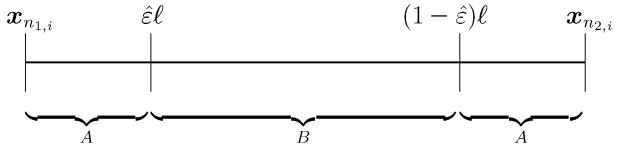

Fig. 1. Fluid edge of length ℓ that is subdivided into parts A and B depending on $\hat{\varepsilon}$. If the fluid edge is intersected in part A then the closest fluid node is shifted, if part B is dissected then a new fluid node is added.

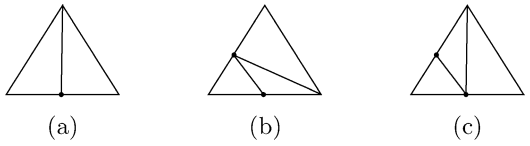

Fig. 2. Different configurations for subdividing tetrahedrons with 1 intersection into 2 triangles (a), with 2 intersections into 3 triangles (b) and (c).

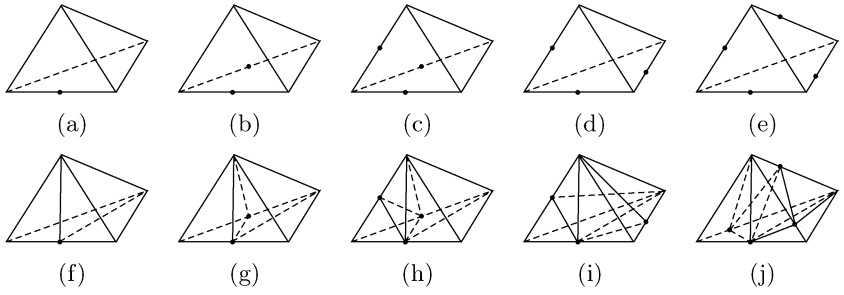

Fig. 3. Basic configurations for tetrahedrons with 1 intersection (a), 2 intersections (b), 3 intersections (c), (d), and 4 intersections (e). Extra edges are created by subdividing the triangular faces. Since there are two ways of subdividing a face with two intersected edges, many tetrahedron subdivisions are possible, but for each configuration (a)–(e) one example is given (f)–(j), respectively.

The arbitrary parameter $0 < \hat{\epsilon} \leqslant 0.5$ should be defined by the user and is explained graphically in Fig. 1. After defining these three sets of edges the actual adaptation of the mesh can be initiated, by first repositioning and adding nodes such that,

$$\begin{aligned}
&\boldsymbol{x}_{n_{1,i}} = \boldsymbol{x}_i, \quad \text{with } \boldsymbol{x}_i \in X_i,\ \forall i \in S^{f1}\\
&\boldsymbol{x}_{n_{2,i}} = \boldsymbol{x}_i, \quad \text{with } \boldsymbol{x}_i \in X_i,\ \forall i \in S^{f2}\\
&\hat{\boldsymbol{x}}_{\hat{n}_i} = \boldsymbol{x}_i, \quad \text{with } \boldsymbol{x}_i \in X_i,\ \forall i \in S^{f3}
\end{aligned}$$

in which $\hat{\boldsymbol{x}}_{\hat{n}_i}$ is the position of a newly created node $\hat{n}_i$ on edge Γ_i^f. With respect to the repositioning of the beginning or ending point of an edge, we impose that the position of a node is allowed to be changed only once, even if this node is shared by several intersected edges.

By adding new nodes, a cascade in topological changes takes place in the fluid mesh. Every edge Γ_i^f, with a newly created node at the intersection point, will be subdivided into two new edges, $\widehat{\Gamma}_{i,1}^f$ and $\widehat{\Gamma}_{i,2}^f$, such that,

$$\begin{aligned}
\widehat{\Gamma}_{i,1}^f &= \left\{\boldsymbol{x} \in \Omega^f\colon \boldsymbol{x} = (1-\alpha)\boldsymbol{x}_{n_{1,i}} + \alpha\hat{\boldsymbol{x}}_{\hat{n}_i},\ 0 \leqslant \alpha \leqslant 1\right\}\\
\widehat{\Gamma}_{i,2}^f &= \left\{\boldsymbol{x} \in \Omega^f\colon \boldsymbol{x} = (1-\alpha)\hat{\boldsymbol{x}}_{\hat{n}_i} + \alpha\boldsymbol{x}_{n_{2,i}},\ 0 \leqslant \alpha \leqslant 1\right\}
\end{aligned}$$

Depending on the number of intersections (one or two per face), an elemental face can be subdivided into two or three subfaces as shown in Fig. 2. Note that there are two different ways of dividing a face into three subfaces (Fig. 2(b), 2(c)), one of which can be chosen arbitrarily (or based on, for example, angles). With respect to the tetrahedral elements, we consider five different configurations one of which can always be obtained by rotation of an intersected element (Fig. 3(a)–(e)). More configurations are thinkable but in case surface γ^s is smooth these will not occur and therefore will not be treated here. Depending on the number and distribution of the intersections over a tetrahedron, two to six new non-overlapping subtetrahedrons will be created that replace the old tetrahedron. The

edges of these tetrahedrons will be straight and the sum of their volumes will be equal to the volume of the original tetrahedron. Every single subface will be the face of a newly created tetrahedron. As mentioned earlier, there are different ways of creating new subfaces and hence there are many different solutions for subdividing a tetrahedron into subtetrahedrons. For each of the presented configurations (Fig. 3(a)–(e)) a corresponding example is shown in Fig. 3(f)–(j). Note that for small values of parameter $\hat{\epsilon}$ more new elements will be created in the new mesh denoted by ${}^{\Omega}S^{f*}$. However, the created elements will be increasingly ill-shaped. Now, using the elemental faces $\Lambda_i^f \subset \Omega^f$, of the adapted fluid mesh, the new subdomain $\gamma^f \subset \Omega^f$ can be defined as,

$$\gamma^f = \left\{ \boldsymbol{x} \in \Lambda_i^f \colon \boldsymbol{x}_{n_{1,i}} \in \gamma^s,\ \boldsymbol{x}_{n_{2,i}} \in \gamma^s,\ \boldsymbol{x}_{n_{3,i}} \in \gamma^s \right\}, \quad \forall i \in {}^{\Lambda}S^{f*} \tag{8}$$

where $n_{1,i} \in {}^{x}S^f$, $n_{2,i} \in {}^{x}S^f$ and $n_{3,i} \in {}^{x}S^f$ are the nodes at the vertices of a triangular face Λ_i^f. Since γ^s is part of the solid, which moves through the fluid domain during computations, domain γ^f, which is based on γ^s, will also change every time step.

2.2.2. Elements

For the three-dimensional model problems discussed in Section 3, the 15 noded quadratic tetrahedrons ($P_2^+ - P_1$) and 27 noded quadratic hexahedrons ($Q_2^+ - Q_1$) of the Crouzeix–Raviart family are used [20,21]. For the two dimensional model problems their 2D equivalents are used, i.e. the 7 noded triangle for the fluid and the 9 noded quadrilateral for the solid. For all of these elements the pressure is enforced to be continuous inside an element but can be discontinuous from one element to another. This property will be shrewdly used for capturing a moving pressure discontinuities in the fluid domain as will be demonstrated in the next section.

The fluid mesh and solid mesh are generated independently from each other. The solid is modelled with an updated Lagrangian formulation which results in an update of the material points of the mesh every time step, i.e. the solid mesh moves across the Eulerian fluid mesh in time. The initially generated fluid mesh ${}^{\Omega}S^f$ is adapted every timestep to the new position of the solid boundary γ^s, creating surface γ^f at which Eq. (7) applies. The adapted mesh ${}^{\Omega}S^{f*}$ is used for the computation and after each time step the position of the solid is updated and a new adapted mesh ${}^{\Omega}S^{f**}$ is created based on ${}^{\Omega}S^f$ and the new position of the solid. Finally, solutions are mapped from ${}^{\Omega}S^{f*}$ to ${}^{\Omega}S^{f**}$ using the basis functions of the tetrahedral elements.

By taking the discretisation of the coupling elements based on the discretisation in ${}^{\Omega}S^{f*}$, the coupling is enhanced, since the number of coupling of elements that are connected to a fluid element is one. Piecewise linear discontinuous basis functions are used to describe the Lagrange multiplier $\boldsymbol{\lambda}$. Care should be taken with respect to the coarseness of the fluid and solid discretisations. The mesh size of the fluid and Lagrange multiplier h^f should not differ too much from the mesh size of the solid h^s. If the ratio $h^f/h^s \ll 1$, accuracy improves but the condition of the algebraic system deteriorates and, vice versa, if $h^f/h^s \gg 1$ the condition of the algebraic system improves but accuracy goes down.

An implicit Euler time integration scheme is used for the solid as well as the fluid. The finite element package SEPRAN [22] is used and extended for building the matrix and mapping the solutions. The set of equations is solved fully coupled, leading to a linear system whos matrix is non-symmetric and sparse. We solve this linear system using a direct method based on a sparse multifrontal variant of Gaussian elimination (HSL/MA41) [23].

3. Numerical experiments

By means of several model problems, the abilities and inabilities of the described method will be analysed. Firstly, a simple plain strain example is presented, showing large rotations and translations of a slender body in a pulsatile fluid flow. Secondly, the shear stresses at both sides of a similar slender body are computed in two different ways. The third model problem considers the axisymmetric modelling of a fluid domain which is halfway divided by a thin solid membrane. A pressure applied to the fluid domain will cause the solid membrane to strain resulting in a sharp pressure drop when the problem reaches equilibrium state. Finally, a three-dimensional problem is presented which mimics the third model problem. The adaptive meshing procedure is highlighted and results are compared to model problem three.

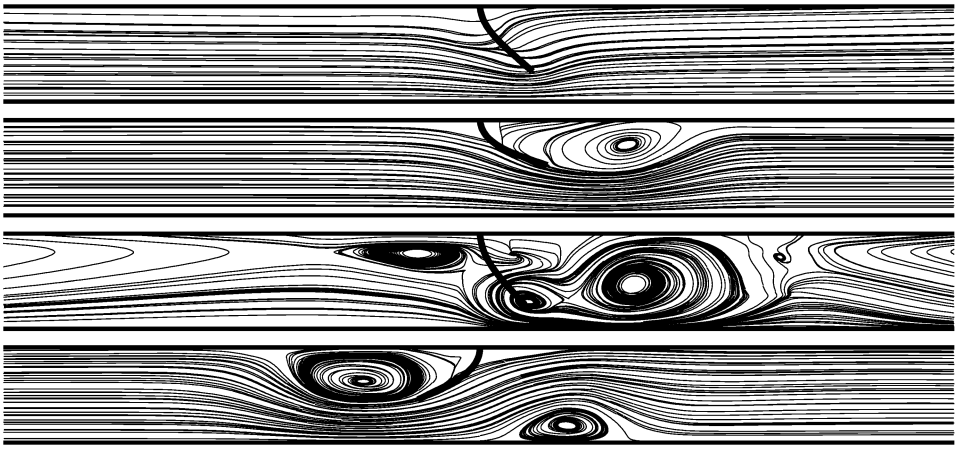

Fig. 4. Streamline plots of the pulsatile fluid flow interacting with a thin solid slab.

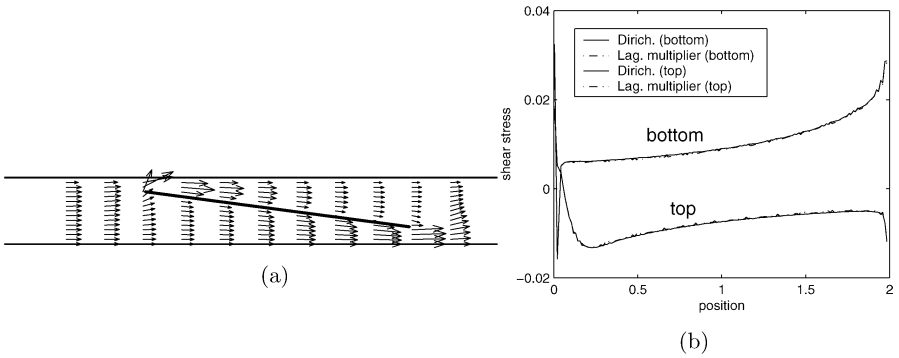

Fig. 5. Vector field of rigid plate in fluid domain (a) and the corresponding shear stress graphs at both sides of the plate (b). The problem is solved once as a fluid–structure interaction model and once as a fluid problem with Dirichlet BC's in a set of internal nodes.

3.1. Model problem 1: motion of a solid slab

A rectangular plain strain fluid domain is considered with no-slip conditions at bottom and top wall. At the inlet the velocity (plug flow) is prescribed as a sinus function of time, which results in a pulsatile flow. The fluid domain is discretised into quadratic triangular elements and the solid domain into quadratic quadrilateral elements. Since a slender body is considered, only one of the solid boundaries is defined as γ^s and the influence of the fluid underneath the fictitious solid body can be neglected. The flow induces the flexible slab, that is attached to the upper fluid wall, to move. The slab in its turn interacts with the fluid which highly influences the flow behaviour as shown by the streamline plots (Fig. 4). In this example the Reynolds number is 1000 based on the height of the channel and the average peak velocity at the inlet. Note that in order to circumvent boundary influences, the height:length ratio of the domain is taken as 20:1. However, very coarse triangulations are used towards the inlet and outlet boundary.

3.2. Model problem 2: shear stresses along a rigid plate

This problem shows the ability of the method to capture the shear stresses at both sides of a slender body. Again a rectangular fluid domain is modelled but now with an immersed stiff solid plate skewly positioned in the middle of this domain (Fig. 5(a)). The same elements are used as in the former problem and again one boundary (in the length of the plate) is defined as γ^s. A stationary solution for the Navier–Stokes equation is found by applying a velocity plug flow at the inlet. The problem is solved twice, once using the method described in this paper, and once by applying homogeneous Dirichlet boundary conditions in all fluid nodes of γ^f and not taking the solid equations into account. For both problems the shear stress is computed at both sides of the solid and the results are compared in

Fig. 5(b). Although the computation with fluid–structure interaction shows some small mesh-dependent oscillations, the differences with the fluid computation are negligible.

3.3. Model problem 3: pressure drop in fluid domain (axisymmetric)

This model is used to emphasise the capability of the method to capture steep pressure gradients inside the fluid domain. A circular fluid domain is considered with a thin solid membrane dividing this domain halfway. This problem can be solved using an axisymmetric model, which results again in a rectangular fluid domain where the upper wall is the symmetry axis. The solid domain is defined from the axis to the bottom wall. The solid as well as the fluid are prohibited from moving/flowing through the axis but are free to move along the axis. The solid is attached to the fluid wall at which a no-slip condition applies. Unlike the former model problems a stress in axial direction is applied depending on time, by taking the first quarter of a sinus function and then keeping the pressure at a constant level such that equilibrium is reached. The fluid will start to flow and the pressure will build up in the left side of the fluid domain inducing the solid to bend (Fig. 6). After some oscillating movement due to inertia forces, solid and fluid reach the equilibrium state. At this point in time the pressure in the left part of the fluid domain will be the applied stress, the pressure in the right part of the domain will be zero and the fluid flow in the whole domain will be zero.

3.4. Model problem 4: pressure drop in fluid domain (3D)

A similar circular fluid domain with thin solid membrane can be modelled in three dimensions. A quarter of the cylinder is discretised in 15 noded quadratic tetrahedral elements, the 3D analogue of the 2D extended quadratic triangles, as used in the former problems. The solid membrane is modelled by defining a mesh consisting of hexahedral elements. The same boundary conditions apply as in the third model problem, which results in a fluid domain with two symmetry edges and a wall with no-slip condition and a solid fixed at the fluid wall. One of the two boundary surfaces of the solid that divide the fluid domain in two parts is taken as γ^s resulting in a fluid surface γ^f after adapting the fluid mesh. In Fig. 7(a) it is clearly seen that these surfaces are non-conformal with respect to each other. As mentioned

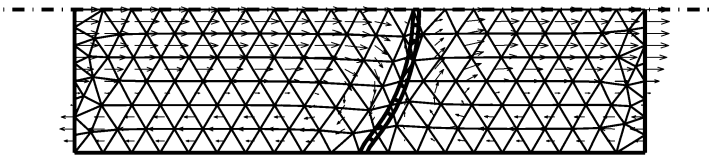

Fig. 6. Axisymmetric model of a solid membrane in a fluid domain with applied pressure at the left wall. The solid stopped moving but the fluid still flows.

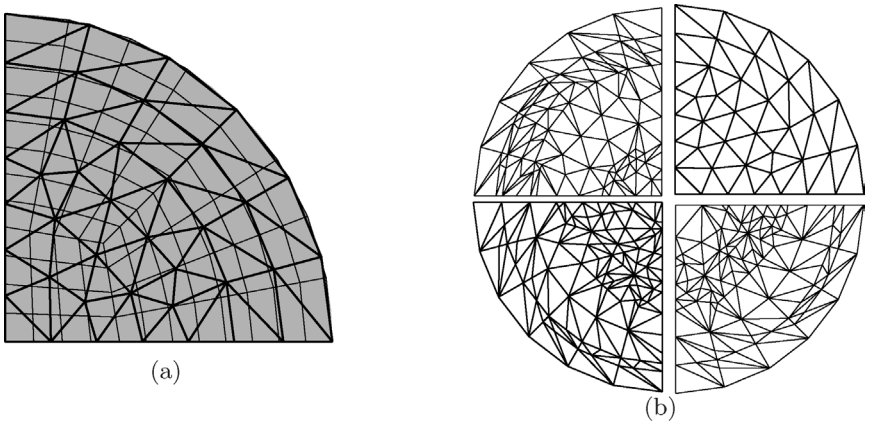

Fig. 7. The non-conformal surfaces γ^s and γ^f, which are part of the fluid and solid mesh, respectively. A Lagrange multiplier is defined over these surfaces by which fluid and solid are coupled (a). Clockcounterwise from the upper right picture, the inner fluid surface, γ^f is shown for time steps $t = 0.6$, $t = 4.8$, $t = 10.8$ and $t = 18$, respectively (b).

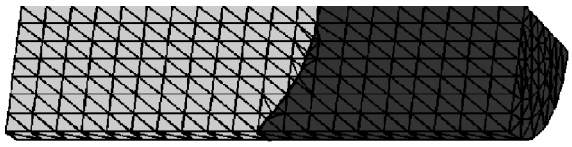

Fig. 8. The solid membrane surface, γ^f, and the newly created inner fluid surface, γ^f.

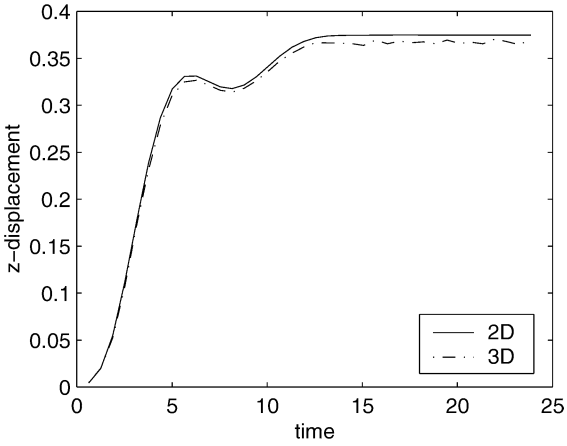

Fig. 9. The z-displacement of the center of the solid membrane as a function of time.

earlier, the position of γ^s changes in time coupling as will surface γ^f, which is based on the intersection of γ^s with the fluid mesh (Fig. 7(b)). As for the axisymmetric example in equilibrium state, the fluid domain is divided into a part with the applied pressure and a part with zero pressure as shown in Fig. 8. By following the time evolution of the point of the membrane located on the axis, we can make a comparison between model problem three and model problem four. The axial displacements are graphically presented as a function of time in Fig. 9. There is hardly any difference in these transients except for the equilibrium position. This is caused by the coarseness of the coupling surface near the axis point in the 3D mesh. The initial solid and fluid mesh consist of 80 and 3600 elements, respectively. During adaptation, with parameter $\hat{\epsilon} = 0.2$, a variation of 200 to approximately 400 fluid elements is added to this number as well as 150 to 175 coupling elements.

4. Conclusion

A method is proposed suitable for modelling the fluid dynamics of a flexible heart valve in a fluid domain. Large rotations and translations of a slender solid body, induced by a pulsatile fluid flow, can be captured at high Reynolds numbers. Furthermore, accurate shear stress information at both sides of the solid can be computed as well as a large pressure gradient across the solid. The potential of the method is demonstrated, considering three 2D and one 3D model problem.

We consider a thin solid body immersed in a fluid domain. The finite element meshes of solid and fluid are generated independently from one another and are therefore non-conformal with respect to each other, which makes meshing easier. Both domains are coupled by applying a Lagrange multiplier along the boundary of the solid, which enforces the interpolated fluid and solid velocities to be equal. In addition, an adaptive meshing scheme is introduced, which adapts the fluid mesh to the position of the solid. This mesh adaptation is only applied locally, only near the position of the solid and is computationally inexpensive and robust since the fluid and solid mesh do not have to be conformal. Furthermore, steep pressure gradients across the solid can be captured, making use of the discontinuous pressure description of the quadratic fluid elements. Similarly, gradients of the velocity and therefore shear stresses can be discontinuous. In this paper, the mathematical formulation is presented in 3D, but demonstrated using 2D and 3D model problems.

Before the methodology, as presented here, can be used for analysing heart valve dynamics, some critical points should be addressed first. Although different model problems show situations analogue to systole and diastole, a

combination is not yet possible. In order to model the closing behaviour of a valve, a contact algorithm is needed. Furthermore, the computing time for 3D problems is very large, which leads to concessions in mesh resolution. However, the boundary layer, that scales with $1/\sqrt{Re}$, will become very small at the leaflet, making it very hard to compute shear stresses accurately. The cure for this problem can be sought in different areas: for example more appropriate solver could be used for solving the fully coupled set of equations. Currently, iterative solvers like GMRES and CG with an incomplete LU decomposition need much fill-in in order to converge and the direct solver used in this paper is also clearly not ideal. Another way of saving CPU time, would be a more efficient way of meshing. The adaptive meshing could be extended such that the element size in the vicinity of the solid can be reduced to a level with which shear stresses can be computed accurately. Finally, more efficient alternatives should be found for the fifteen noded tetrahedrons.

Acknowledgements

This research is performed in the scope of the Hemodyn project, which is a cooperation between Philips Medical Systems Best, the Technical University Eindhoven and the Erasmus University Rotterdam, the Netherlands. It is financially supported by Senter (Dutch Ministry of Economic Affairs) in their TS subsidy programme (Technologische Samenwerking).

References

[1] C.S. Peskin, Flow patterns around heart valves: a numerical method, J. Comput. Phys. 10 (1972) 252–271.
[2] C.S. Peskin, The immersed boundary method, Acta Numer. 11 (2002) 479–517.
[3] C.S. Peskin, D.M. McQueen, A three-dimensional computational method for blood flow in the heart I. Immersed elastic fibers in a viscous incompressible fluid. The immersed boundary method, J. Comput. Phys. 81 (1989) 372–405.
[4] D.M. McQueen, C.S. Peskin, Shared-memory parallel vector implementation of the immersed boundary method for the computation of blood flow in the beating mamalian heart, J. Supercomp. 11 (1997) 213–236.
[5] V.B. Makhijani, H.Q. Yang, P.J. Dionne, M.J. Thubrikar, Three-dimensional coupled fluid–structure simulation of pericardial bioprosthetic aortic valve functioning, ASAIO J. 43 (5) (1997) 387–392.
[6] C.W. Hirt, A.A. Amsden, J.L. Cook, An arbitrary Lagrangian–Eulerian computing method for all speeds, J. Comput. Phys. 14 (1974) 227–253.
[7] T.J.R. Hughes, W.K. Liu, T. Zimmerman, Lagrangian–Eulerian finite element formulation for incompressible viscous flow, Comput. Methods Appl. Mech. Engrg. 29 (1981) 329–349.
[8] J. Donea, S. Giuliani, J.P. Halleux, An arbitrary Lagrangian–Eulerian finite element method for transient dynamic fluid–structure interactions, Comput. Methods Appl. Mech. Engrg. 33 (1982) 689–723.
[9] M.A. Nicosia, R.P. Cochran, D.R. Einstein, C.J. Rutland, K.S. Kunzelman, A coupled fluid–structure finite element model of the aortic valve and root, J. Heart Valve Disease 12 (2003) 781–789.
[10] J. de Hart, G.W.M. Peters, P.J.G. Schreurs, F.P.T. Baaijens, A three-dimensional computational analysis of fluid–structure interaction in the aortic valve, J. Biomech. 36 (1) (2003) 103–112.
[11] J. de Hart, G.W.M. Peters, P.J.G. Schreurs, F.P.T. Baaijens, A computational fluid–structure interaction analysis of a fiber-reinforced stentless aortic valve, J. Biomech. 36 (5) (2003) 699–712.
[12] J. de Hart, G.W.M. Peters, P.J.G. Schreurs, F.P.T. Baaijens, Collagen fibers reduce stresses and stabilize motion of aortic valve leaflets during systole, J. Biomech. 37 (2004) 303–311.
[13] R. Glowinski, T.-W. Pan, J. Périaux, A Lagrange multiplier/fictitious domain method for the numerical simulation of incompressible viscous flow around moving rigid bodies: (I) case where the rigid body motions are known a priori, C. R. Acad. Sci. Paris 25 (5) (1997) 361–369.
[14] R. Glowinski, Finite element methods for incompressible viscous flow, in: P.G. Ciarlet, J.L. Lions (Eds.), Handbook of Numerical Analysis, vol. IX, North-Holland, Amsterdam, 2003, 3-1176.
[15] F. Bertrand, P.A. Tanguy, F. Thibault, A three-dimensional fictitious domain method for incompressible fluids flow problems, Int. J. Numer. Methods Fluids 25 (6) (1997) 719–736.
[16] F.P.T. Baaijens, A fictitious domain/mortar element method for fluid–structure interaction, Int. J. Numer. Methods Fluids 35 (7) (2001) 743–761.
[17] N.A. Patankar, P. Singh, D.D. Joseph, R. Glowinski, T.W. Pan, A new formulation of the distributed Lagrange multiplier/fictitious domain method for particulate flows, Int. J. Multiphase Flow 26 (9) (2000) 1509–1524.
[18] J.M.A. Stijnen, J. de Hart, P.H.M. Bovendeerd, F.N. van de Vosse, Evaluation of a fictitious domain method for predicting dynamic response of mechanical heart valves, J. Fluid Struct. 19 (2004) 835–850.
[19] R. van Loon, P.D. Anderson, J. de Hart, F.P.T. Baaijens, A combined fictitious domain/adaptive meshing method for fluid–structure interaction in heart valves, Int. J. Numer. Methods Fluids 46 (2004) 533–544.
[20] V. Girault, P.A. Raviart, Finite Element Approximation of the Navier–Stokes Equations, Lecture Notes in Math., vol. 749, Springer-Verlag, New York, 1979.
[21] F. Brezzi, M. Fortin, Mixed and Hybrid Finite Element Methods, Springer-Verlag, 1991.

[22] G. Segal, SEPRAN Introduction, User's Manual, Programmer's Guide and Standard Problems, Ingenieursbureau SEPRA, Leidschendam, 2003.
[23] HSL(2002), A collection of Fortran codes for large scale scientific computation, http://www.numerical.rl.ac.uk/hsl.